3. Microstructure, Texture, Mechanical and Ballistic Properties Correlation of a Hot-rolled and Peak Aged AA 7017 Plate at Surface and Centre

3.1. Introduction

This Chapter focuses on the understanding of the effect of through thickness anisotropy on mechanical and ballistic behaviour of a 70 mm thick AA 7017 alloy plate. The ballistic behaviour of the 70 mm thick AA 7017 alloy plate has been evaluated by impacting on its surface and centre. The ballistic results have been correlated with the microstructure and texture of the plate at its surface and centre. Related damage and microstructure of the material after ballistic impact have also been analyzed. In addition, a comparative study of the mechanical properties has been carried out to explain the ballistic behaviour.

3.2. Results

3.2.1. Initial microstructure

The optical microstructures of the plate at the surface and centre are shown in Fig. 3.1. This exhibits three distinct features namely grey matrix, white region along grain boundaries and dark precipitates. The white regions reflect the particle simulated nucleated (PSN) recrystallized grains. The recrystallization occurs around intermetallic precipitates due to the presence of larger strains at the interface between precipitates and matrix (Ko, 2014). The volume fraction of recrystallized grain is comparatively large at the surface in comparison to that of the centre of the plate. The back scattered electron (BSE) image of the plate displays the presence of two types of precipitates with bright and dark contrasts

(Fig.3.2). The analyzed compositions obtained by EPMA indicate that these are Al_6FeMn and Mg_2Si precipitates (Table 3.1).

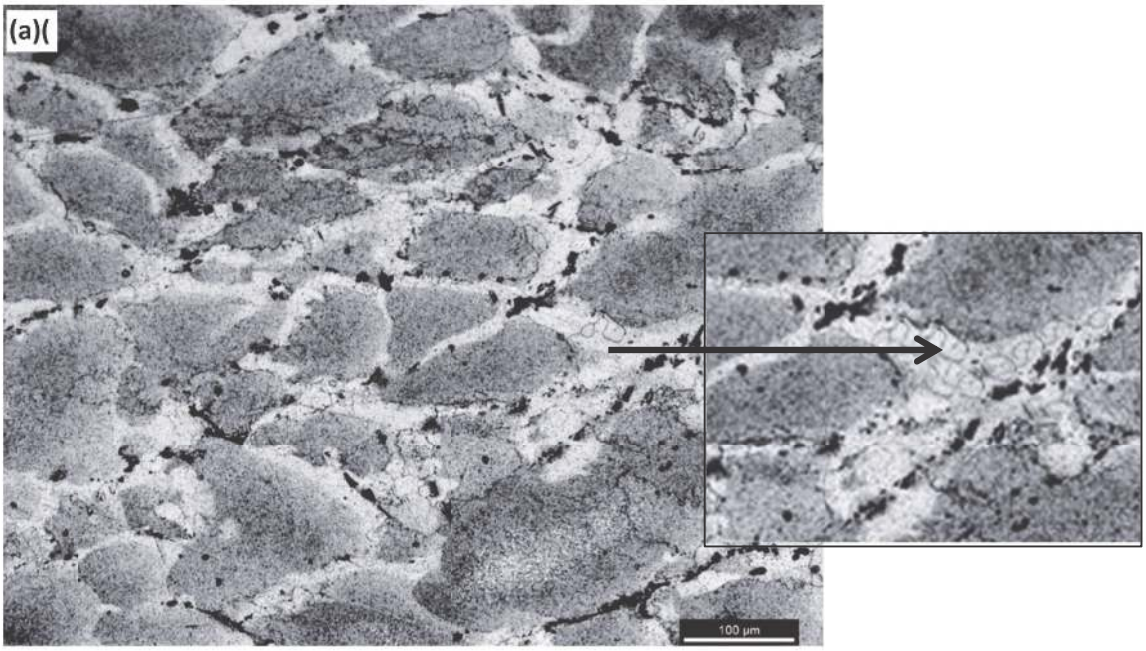

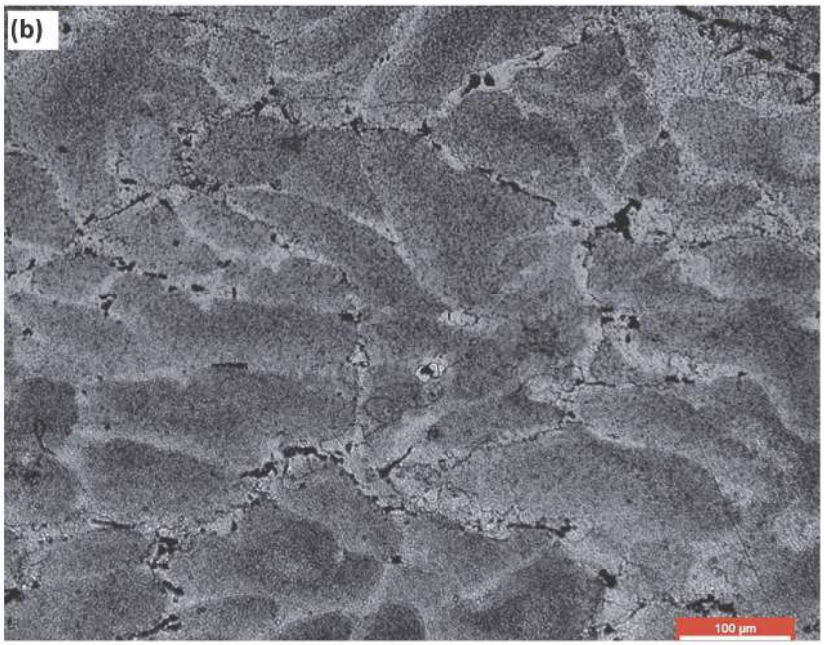

Fig. 3.1: Optical microstructures of the normal direction planes taken from (a) surface and (b) centre of the 70 mm thick plate.

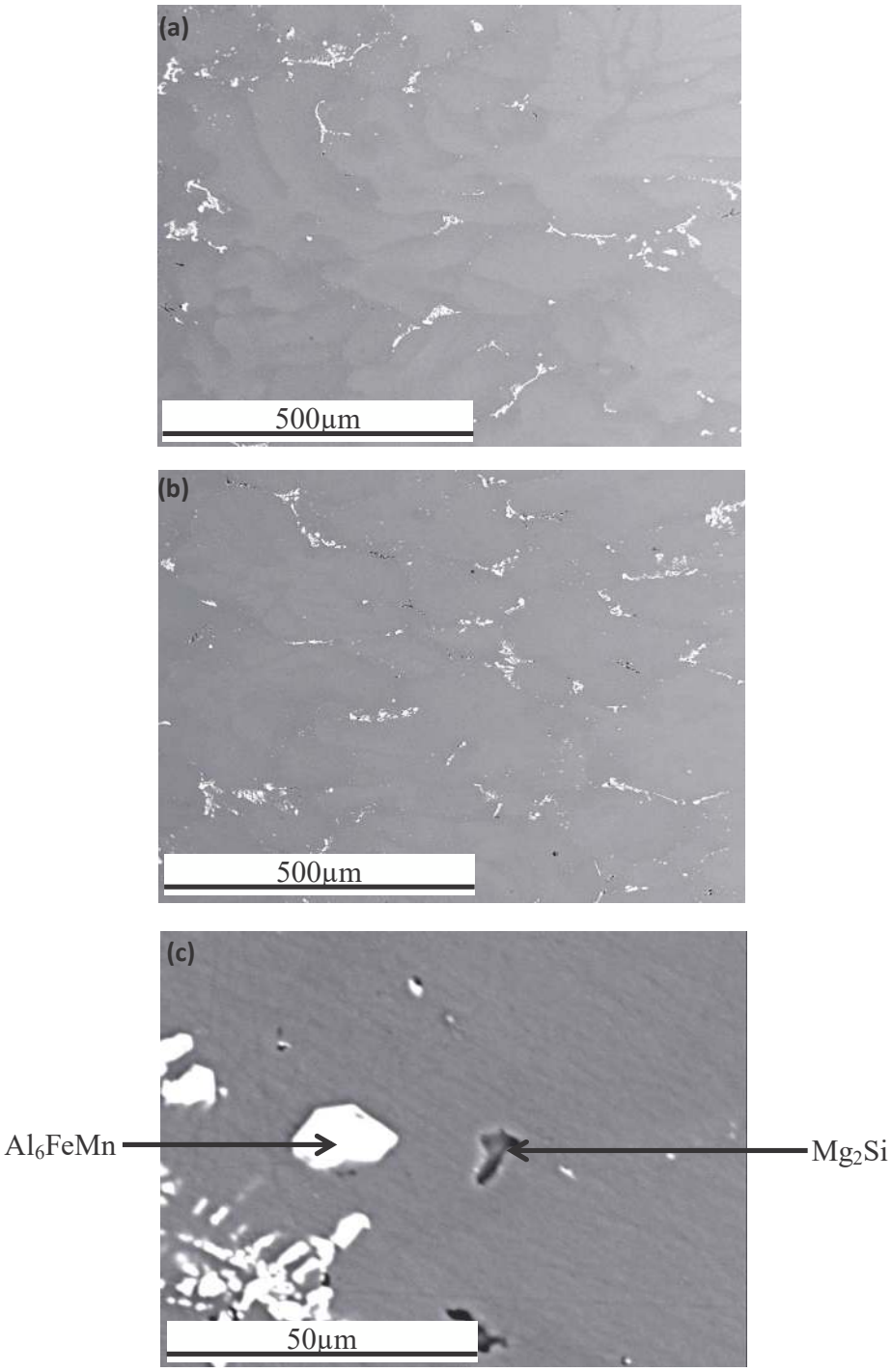

Fig 3.2: BSE microstructure taken from the (a) surface, (b) centre of plate and (c) BSE microstructure showing white (Al_6FeMn) and dark contrast (Mg_2Si) precipitates.

Table 3.1.Analyzed compositions of the precipitates by EPMA.

Weight %	Mg	Al	Si	Cr	Mn	Fe	Zn	Total
Bright	0.32	72.91	0.46	0.19	11.85	12.38	1.33	99.43
Gray	63.16	3.68	29.79	0.04	0.03	0.04	3.01	99.75

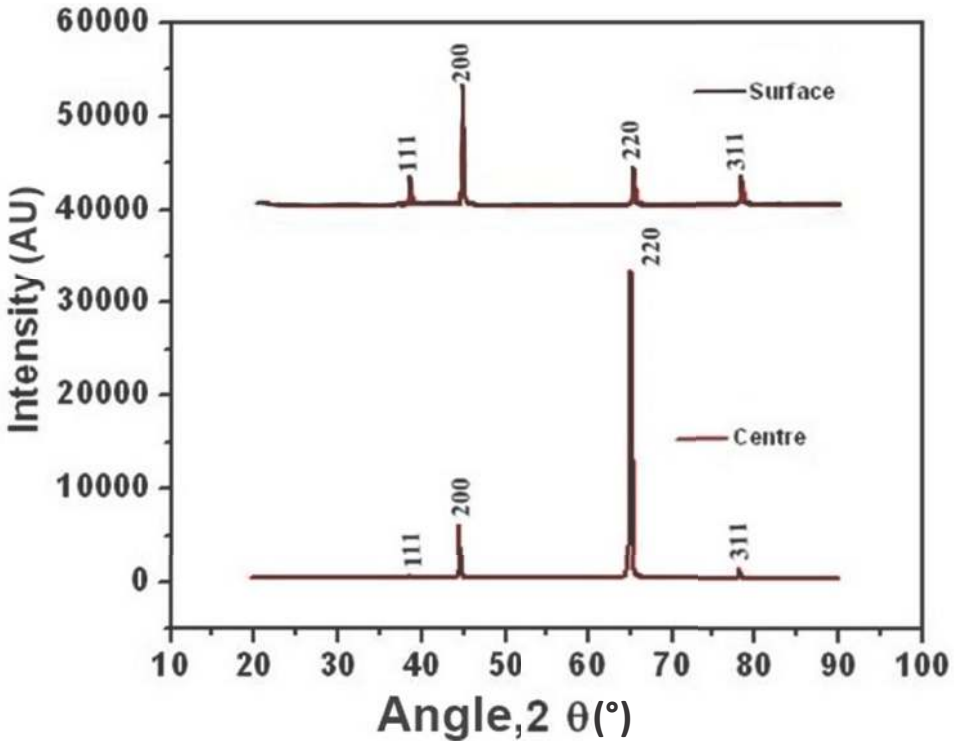

Fig. 3.3: XRD patterns taken from the surface and centre of the 70 mm thick plate.

3.2.2. Texture characterization

The XRD pattern of the alloy shows that the matrix is typical face-centered-cubic (fcc) phase (Al matrix, $Fm\bar{3}m$) (Fig. 3.3). The lattice constant of the matrix phase is 4.05 Å. Peaks corresponding to Al_6FeMn and Mg_2Si precipitates could not be seen owing to less volume fraction of these phases present in the samples. The textures of the materials at the surface and centre are shown in Fig.3.4. The overall intensity of texture at the centre is nearly

7 times larger than that of the surface. The major texture components at the surface and centre of the plate are {0 1 11}⟨3 11 1⟩ [f(g) =1.9], {0 1 11}⟨15 11 1⟩[f(g)=2.5], {0 1 11}⟨8 11 1⟩[f(g)=2.4], {2 0 3}⟨3 0 2⟩[f(g)=2.0], {1 1 4}⟨2 6 1⟩[f(g)= 3.5], {1 1 3}⟨0 3 1⟩[f(g)=2.9], {2 2 1}⟨3 4 2⟩[f(g)=3.3], {1 1 2}⟨1 1 0⟩[f(g)=3.4] and {0 1 1}⟨5 3 3⟩[f(g)=16.4], {4 4 1}⟨1 0 4⟩[f(g)=17.5], respectively. The corresponding typical βfibers of this alloy at centre and surface are shown in Fig.3.5. The β fibre is very weak and homogeneous at the surface while highly inhomogeneous with very high intensity between {168}⟨211⟩ and {011}⟨211⟩ locations.

3.2.3. Mechanical properties

The engineering stress-strain and true stress-true strain curves for the AA 7017 plate at surface and centre are given in Fig.3.6. The average values of yield strength (σ_{YS}), ultimate tensile strength (σ_{UTS}) and elongation at the surface and centre are given in Table 3.2 and Fig. 3.6c. The impact energy values obtained from Charpy impact test are also given in Table 3.2 and Fig.3.6d. VHN hardness profile of as received plate from surface → centre → surface is shown in Fig. 3.7. This exhibits a gradual increase and decrease in hardness values from surface to centre and centre to surface, respectively.

The fracture surfaces of the tensile specimens are quite distinct in samples made from surface and centre of the plate. Both the samples exhibit typical ductile dimples which are fine and shallow at the surface where as coarse and flattened at the center (Fig.3.8 a-b). The high magnification BSE fractographs reveal the presence of cracks within and around Fe rich particles (shown by arrow in Fig.3.8 c) at the surface while centre sample exhibits these cracks within and around Fe rich particles as well as in the matrix (shown by arrow in Fig.3.8 d). The Charpy impact samples exhibit absence and presence of cracks in surface and centre specimens, respectively (Fig.3.9 a-b). The high magnification BSE features are similar to those of tensile specimens (Fig.3.9 c-d)

3.2.4. Ballistic Properties

Ballistic properties in terms of the depth of penetration (DOP) obtained by impacting lead and soft steel projectiles from surface and centre of the plate are shown in Fig. 3.10. It

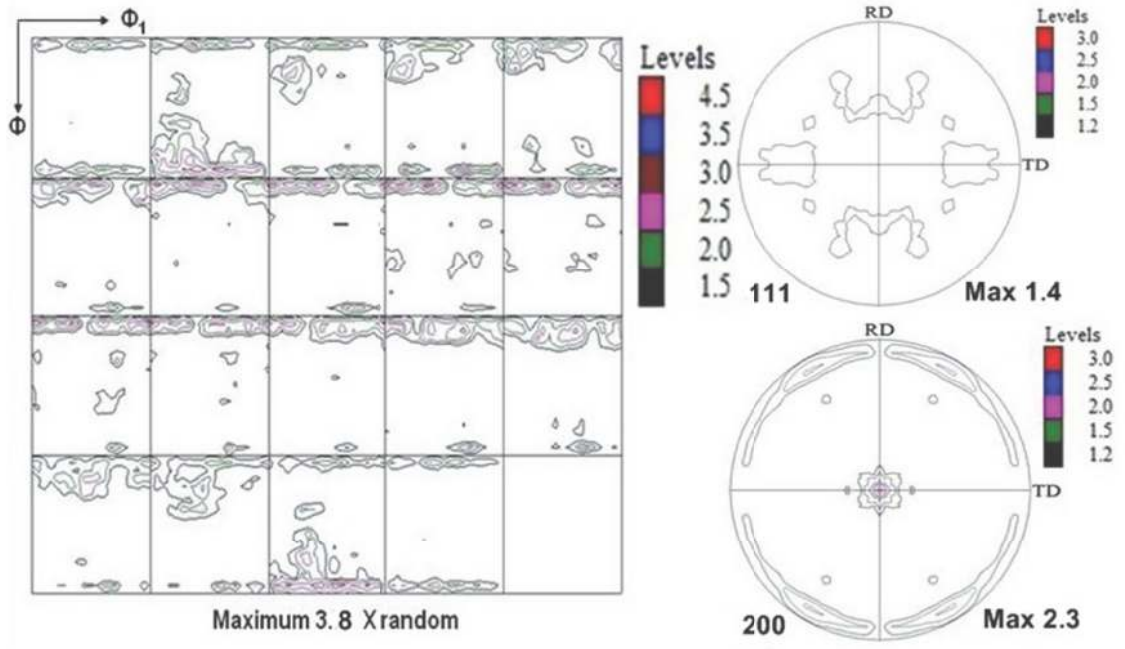

(a)

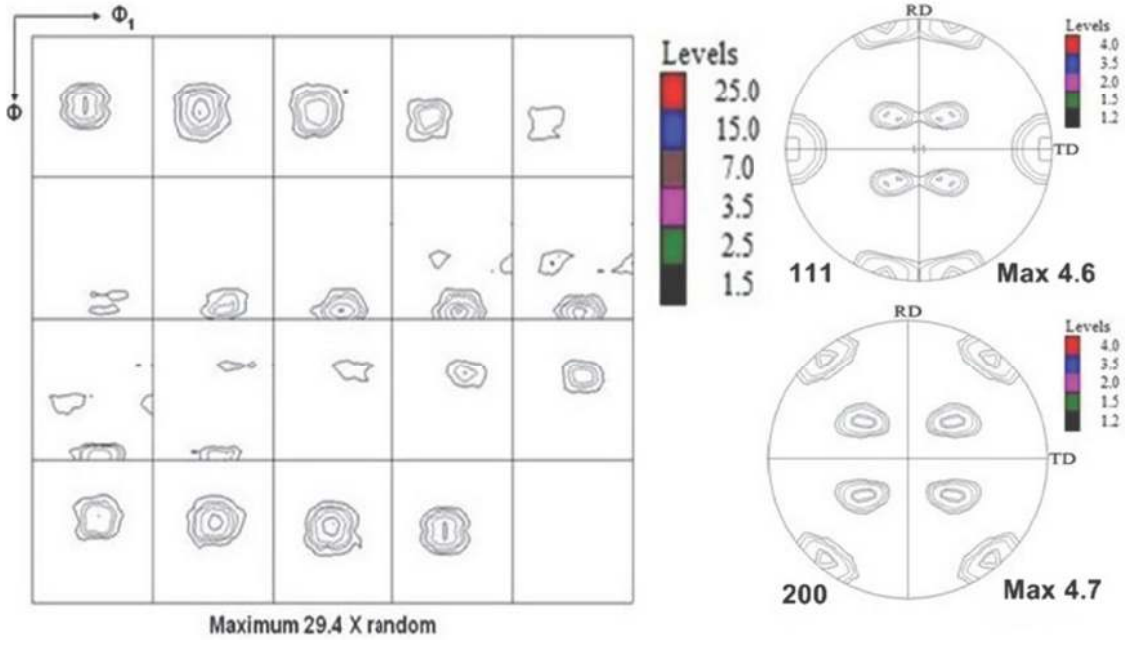

(b)

Fig. 3.4: Textures of the 70 mm thick plate (a) surface and (b) centre.

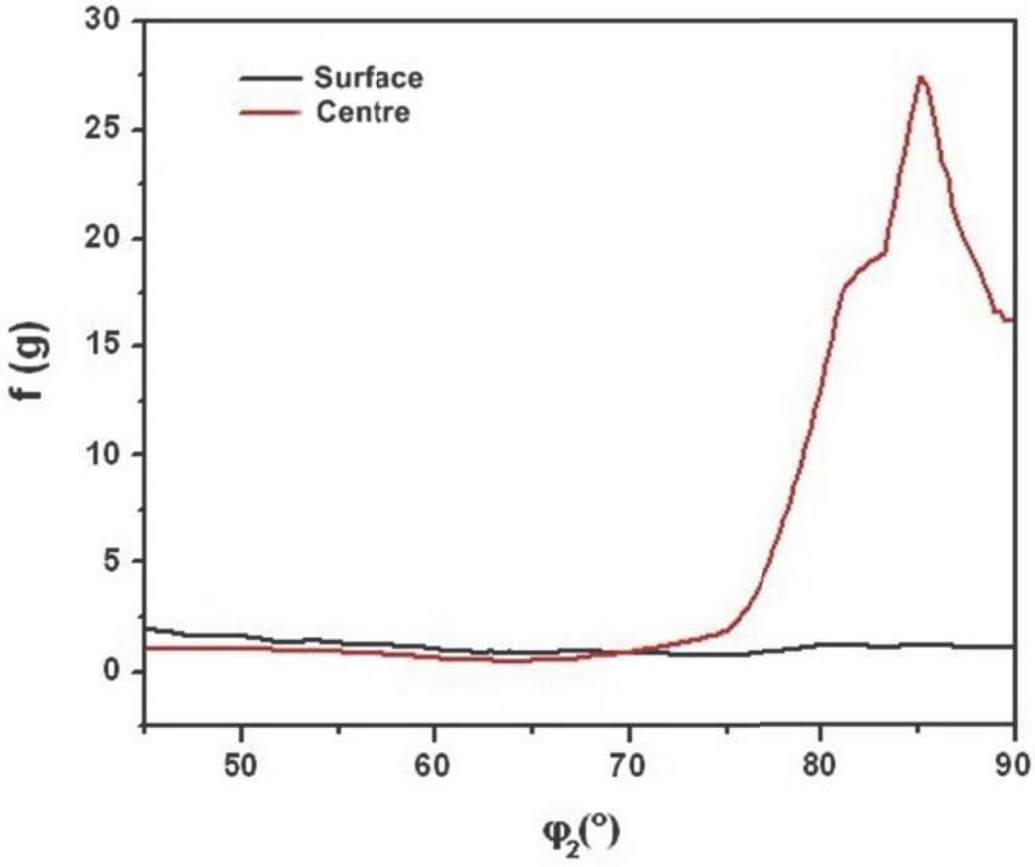

Fig. 3.5: Typical β fibers of surface and centre of the plate.

can be seen that the DOP of plates impacted by both the soft steel and lead projectiles on the centre of the 70 mm AA 7017 plate is higher than that on the surface. It is also observed that the DOP against the soft steel projectile is higher than the lead projectile. The material flows out to form nice petalling damage patterns for the samples impacted on the surface of the 70 mm AA 7017 plate (Fig.3.11a). On the other hand, broken petal damage pattern is observed for the samples impacted on the centre of the 70 mm AA 7017 plate (Fig. 3.11b). The cross sections of the representative post-ballistic impact penetration channels are also included in Fig. 3.11. Macro cracks emanating from the penetration channel are observed for samples impacted on the centre of the 70 mm AA 7017 plate. No such cracks are observed in the samples impacted on the surface of the 70 mm AA 7017 plate.

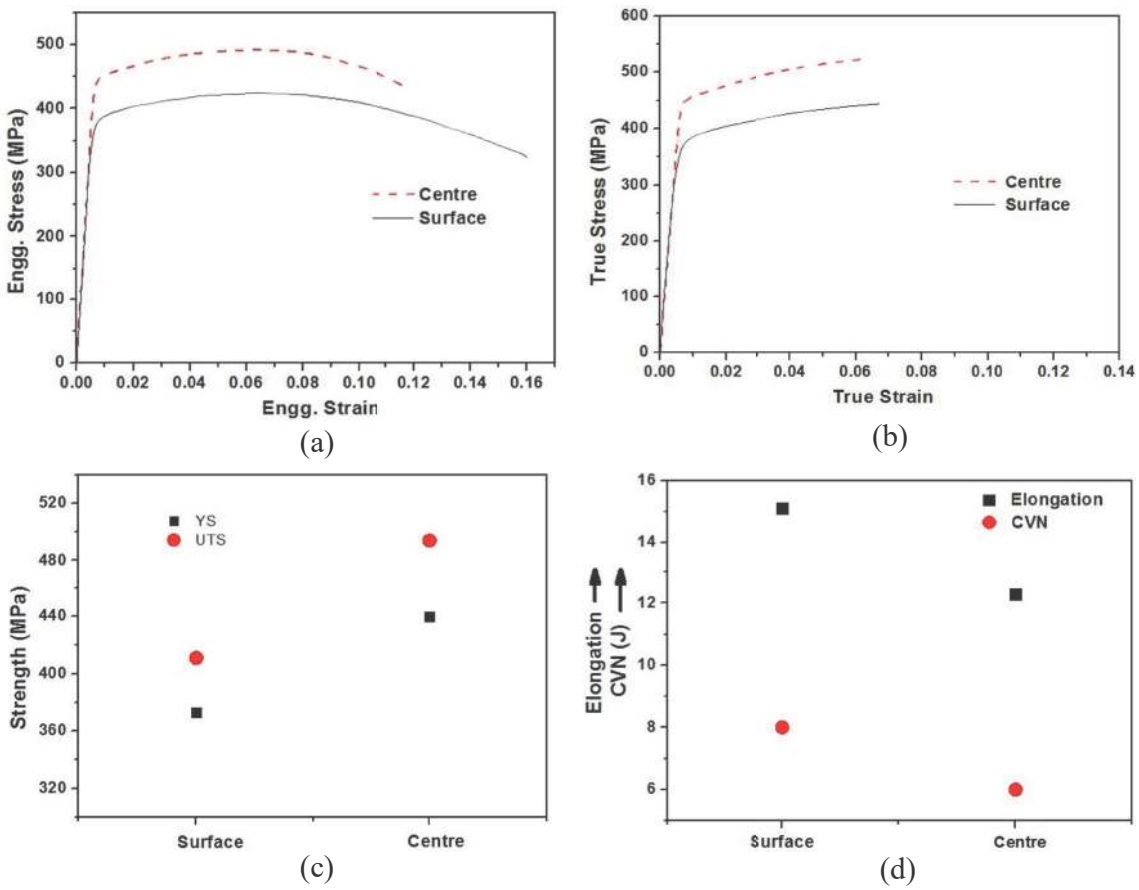

Fig. 3.6: Tensile properties evaluated from the surface and centre of plates: (a) Engineering stress-engineering strain curve, (b) True stress-true strain curve, (c) YS and UTS at surface and centre and (d) CVN and %RA at surface and centre.

Table 3.2. Mechanical properties of the plate at surface and centre ()ADD DEVIATION

Sample location	YS (MPa)	UTS (MPa)	Elongation	CVN (J)
Surface	373	440	15.1	8
Centre	415	496	12.3	6

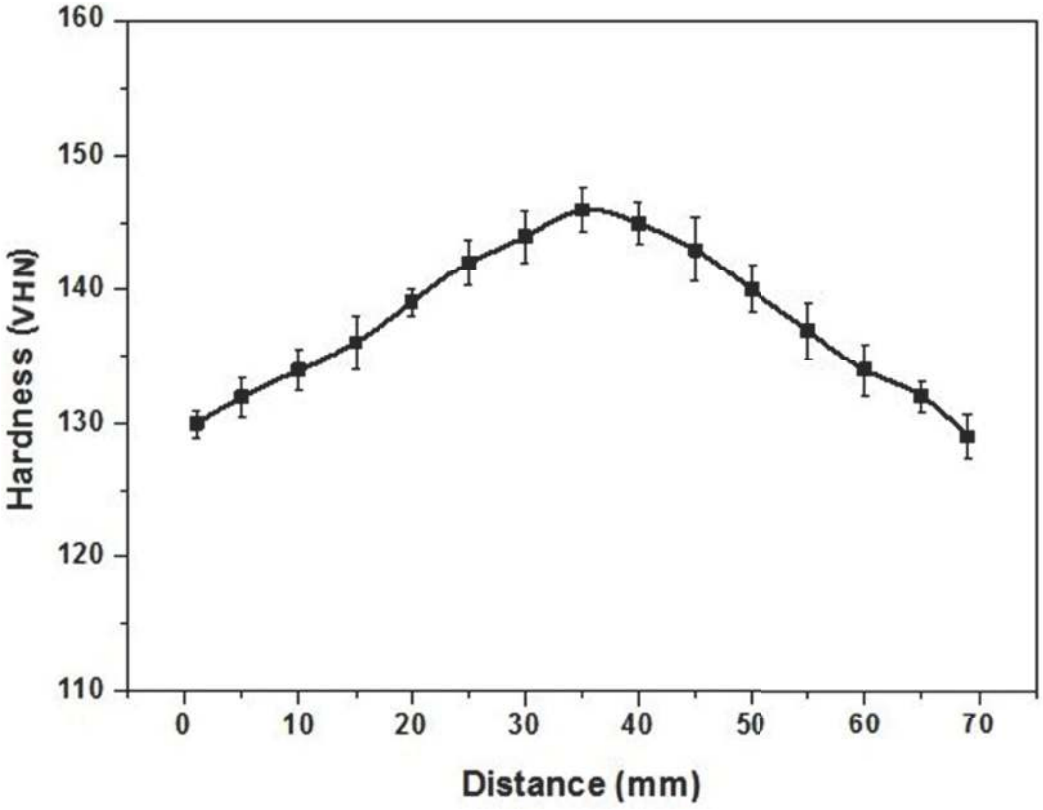

Fig 3.7: Hardness distribution of the plate along the cross section.

3.2.5. Post ballistic microstructure observation

The impact craters have been examined to observe changes in microstructures after ballistic testing. The microstructures of the target impacted on the surface and centre of the AA 7017 plate against lead and soft steel projectiles are shown in Fig 3.12-3.14. The microstructure of the penetration channel formed by the impact of lead projectile on the surface of the AA 7017 plate shows that the material flow lines are severely bent towards the direction of penetration (Fig.3.12a). Only a few shear bands are observed along the penetration channel. Micro-cracks are observed originating from the bottom of the crater. The microstructure of the penetration channel formed by impacting on the centre of the 70 mm AA 7017 plates also reveals material flow lines along with many shear bands

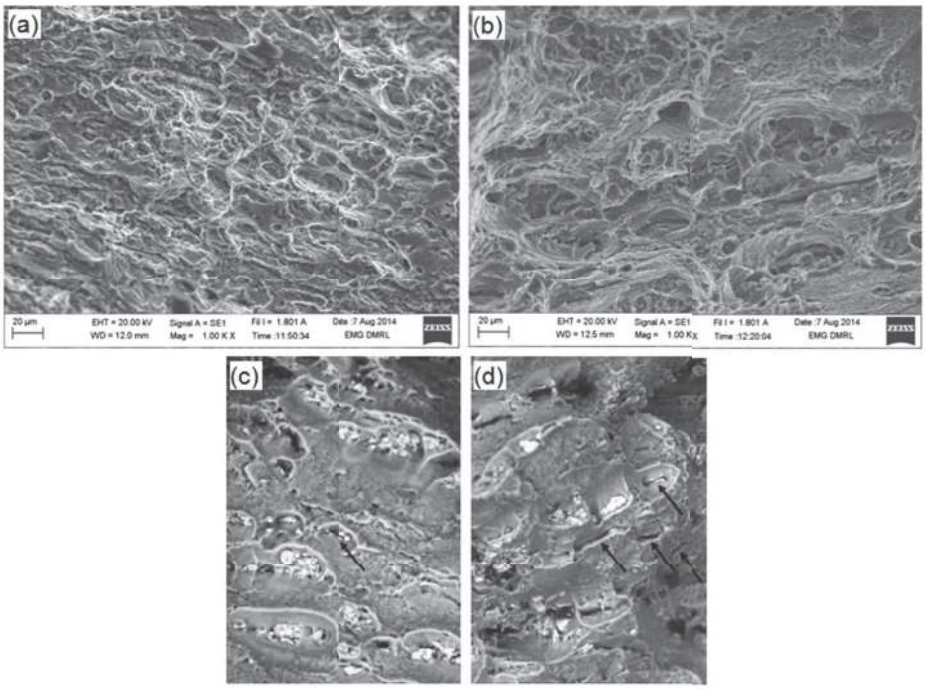

Fig. 3.8: Tensile fractographs (a) surface and (b) centre specimens; Tensile BSE micrographs: (c) surface and (d) centre. Presence of cracks is shown by arrows.

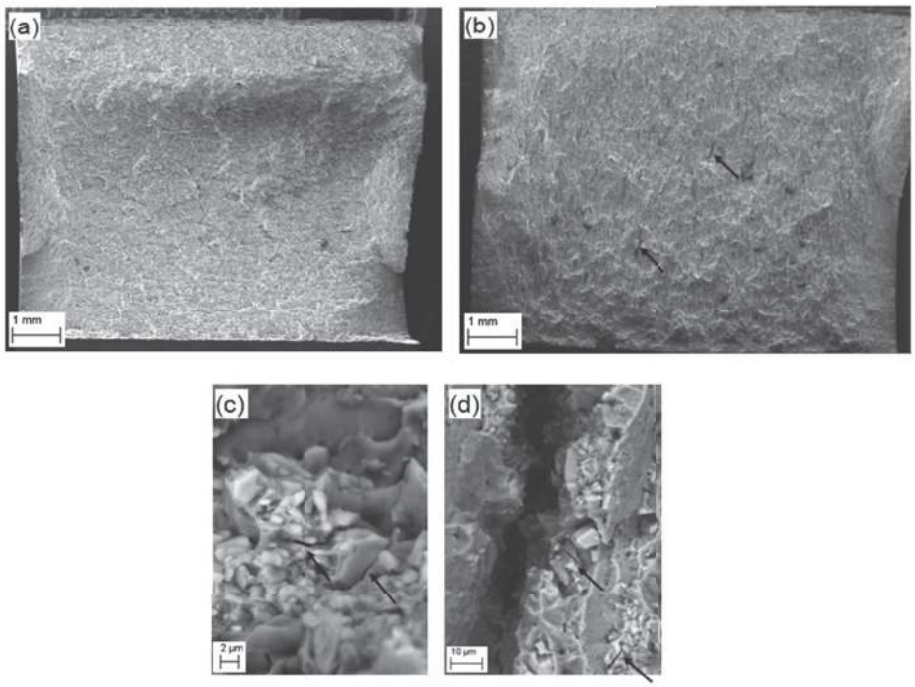

Fig. 3.9: Charpyfractographs (a) surface and (b) centre specimens; Charpy BSE micrographs: (c) surface and (d) centre. Presence of cracks is shown by arrows.

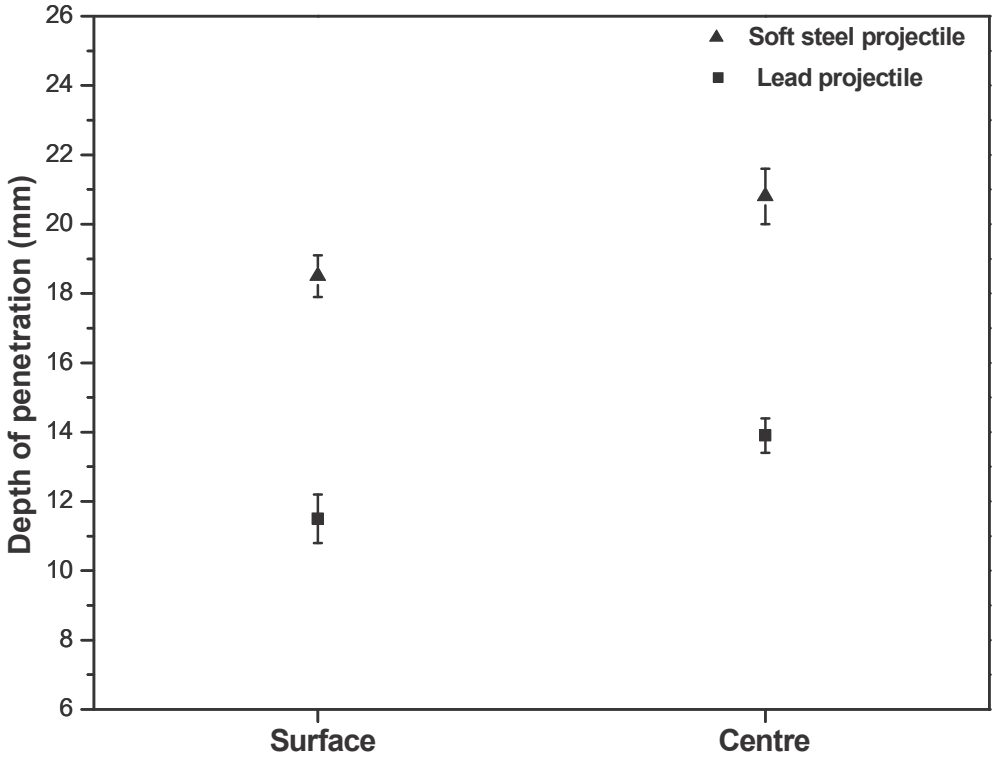

Fig. 3.10: Ballistic results in terms of depth of penetration against lead and soft steel projectiles.

(Fig.3.12b). The number of the shear bands observed to be decreasing towards the bottom of the penetration channel. As seen in Fig. 3.12 b, the adiabatic shear bands (ASB) are connected with cracks, providing an easy crack propagation path. An enlarged view of ASB induced crack has been shown in Fig. 3.13. Cracks are also observed emanating from the bottom of the penetration channel.

The microstructure of the penetration channel formed by the impact of soft steel projectiles on the surface of the 70 mm AA 7017 plates displays that the maximum deformation is observed at the entry of the projectile (Fig. 3.14a). Very few shear bands are seen in the microstructures. A less severe material flow is observed at the bottom of the penetration channel. The penetration channel microstructure of the centre shows severe material deformation at the entry of the projectile (Fig. 3.14b). Similar to the lead projectile impacted microstructures as mentioned above, large numbers of shear bands are observed

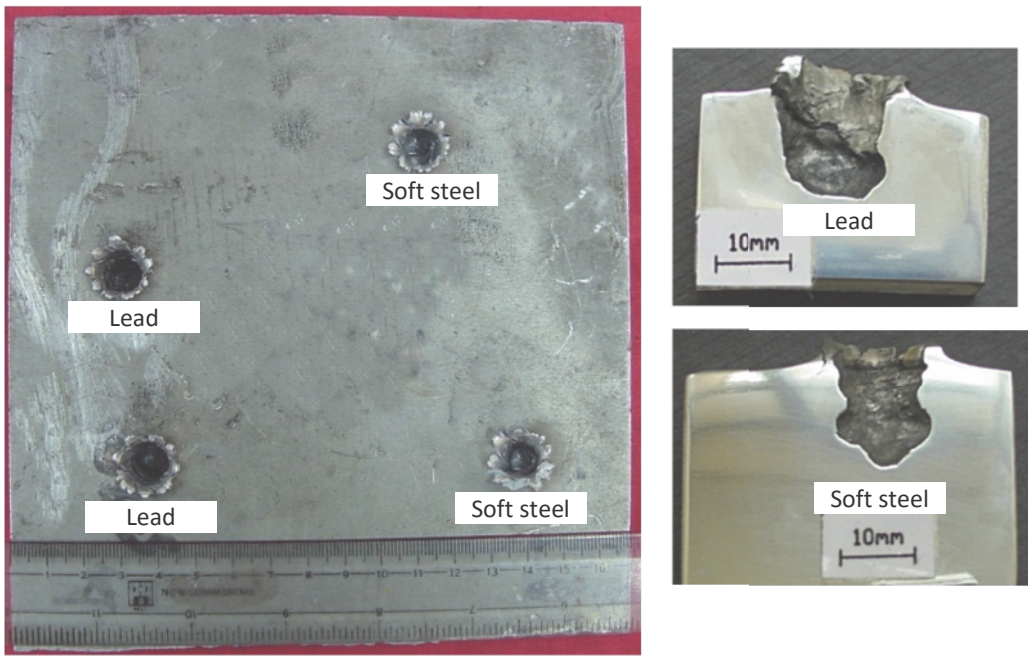

(a)

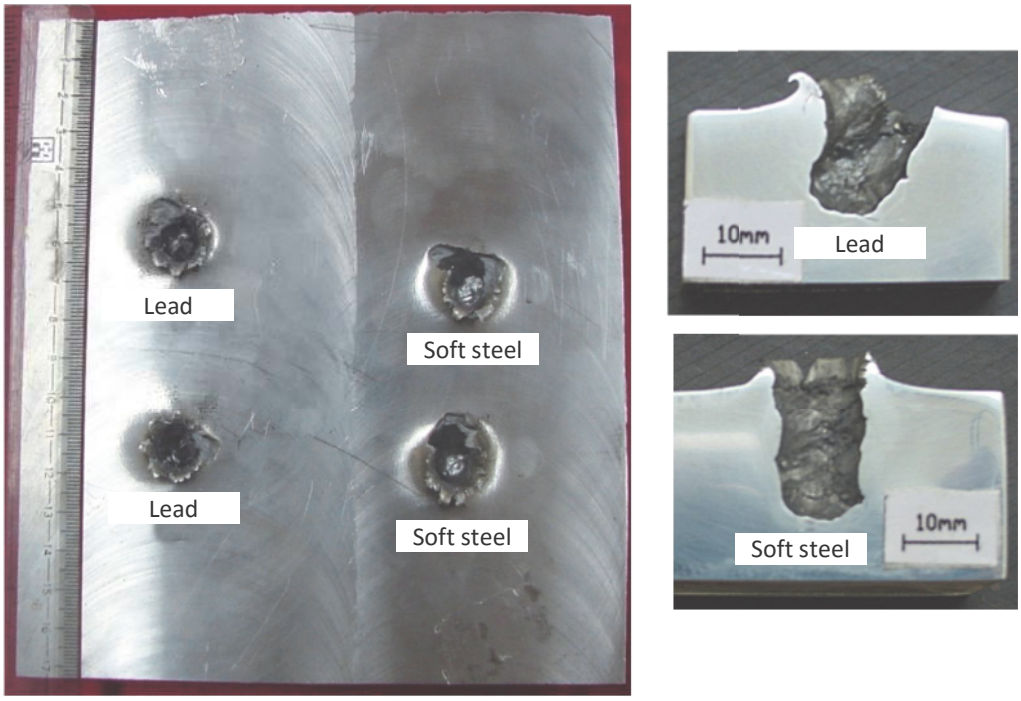

(b)

Fig. 3.11: Front view of the (a) surface and (b) centre plates after ballistic testing. Half section views of the respective penetration channels are also included for comparison.

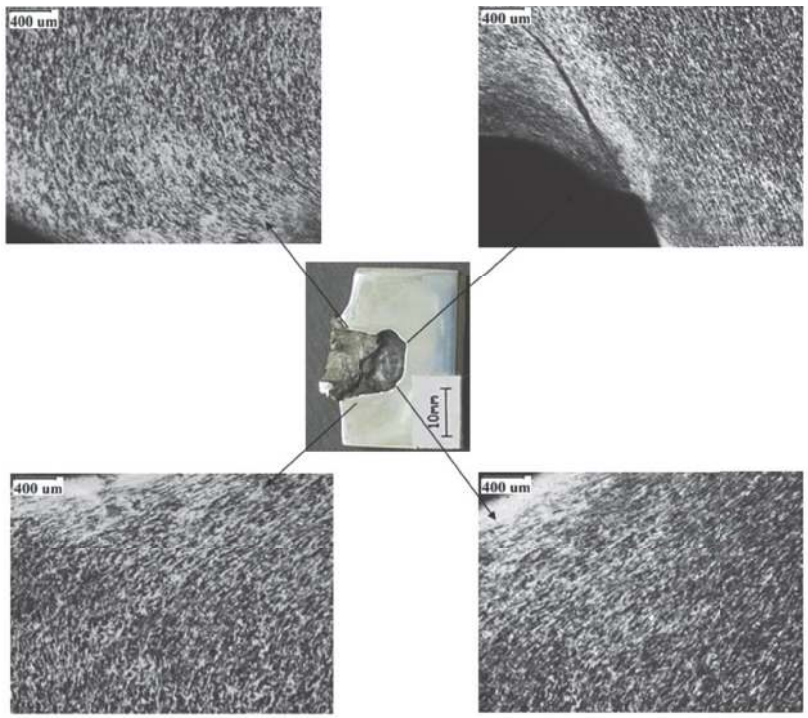

(a)

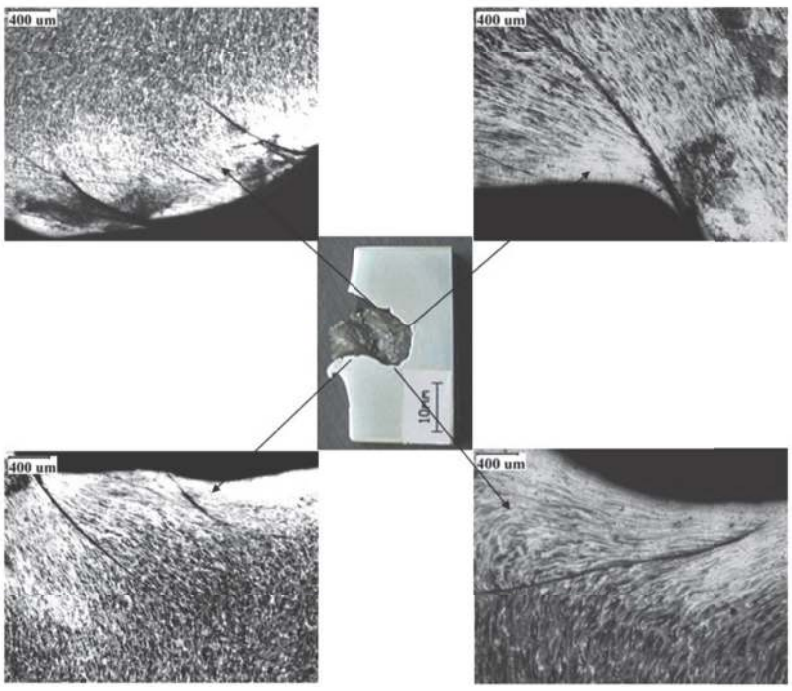

(b)

Fig. 3.12: Post ballistic microstructures along the penetration channel impacted by lead projectile: (a) surface and (b) centre.

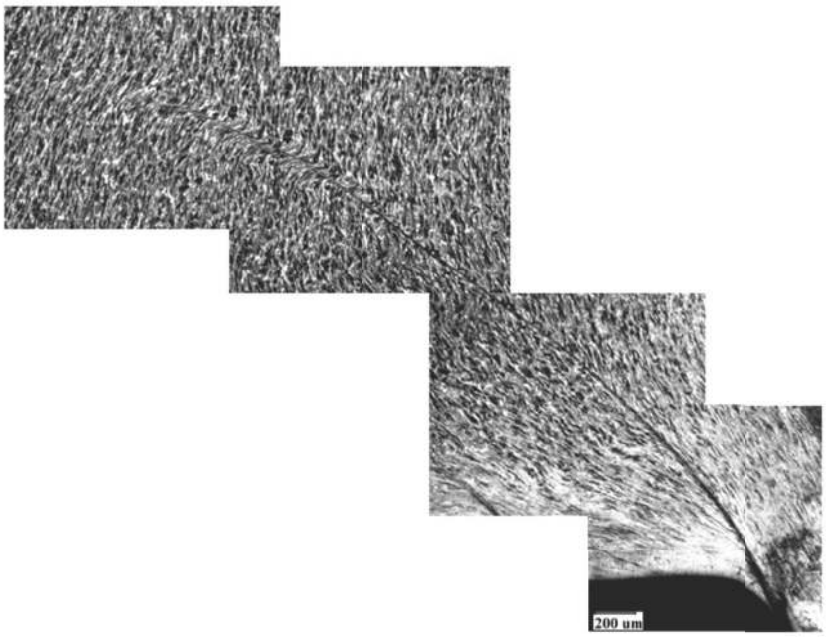

Fig. 3.13: Montage of post ballistic microstructure from the centre showing adiabatic shear bands leading to crack.

along the length of the penetration channel. Micro-cracks are seen emanating from the bottom of the penetration channel.

3.2.6. Post ballistic micro-hardness measurements

In order to examine the deformation process, variation of micro-hardness with the help of Vicker's indenter is measured at 100g load adjacent to the bottom of penetration channel wall created by impact of lead projectiles. Fig. 3.15 summarizes the distribution of hardness along the horizontal direction away from the penetration channel. There is an increase in hardness of all the target plates adjacent to the crater wall compared to the original hardness of the plate. There is a steady increase in the hardness values followed by a gradual decrease in hardness. The region of increase in hardness for the surface impacted targets is more than the targets impacted at the initial centre of the 70 mm AA 7017 plate. In

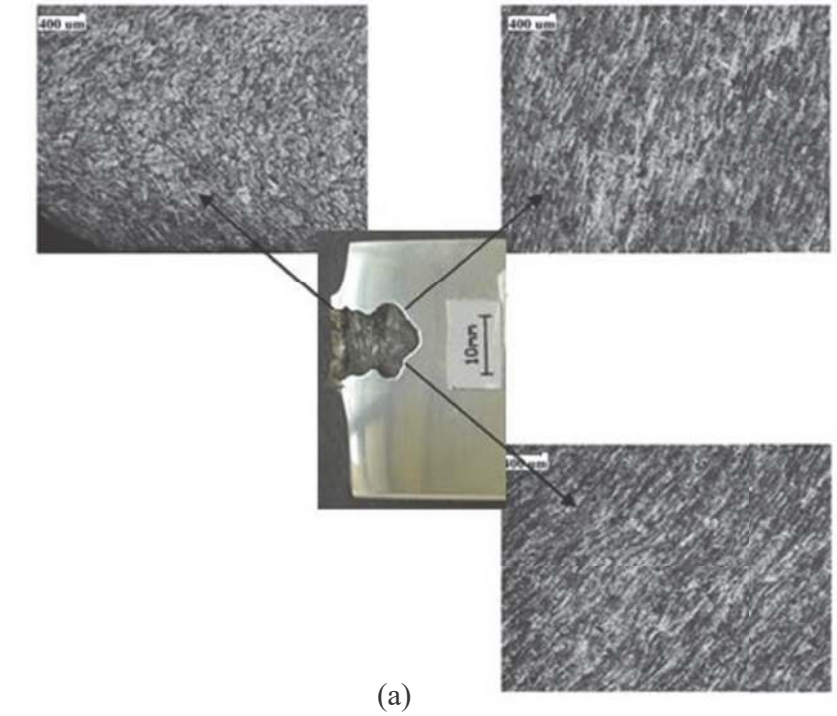

(a)

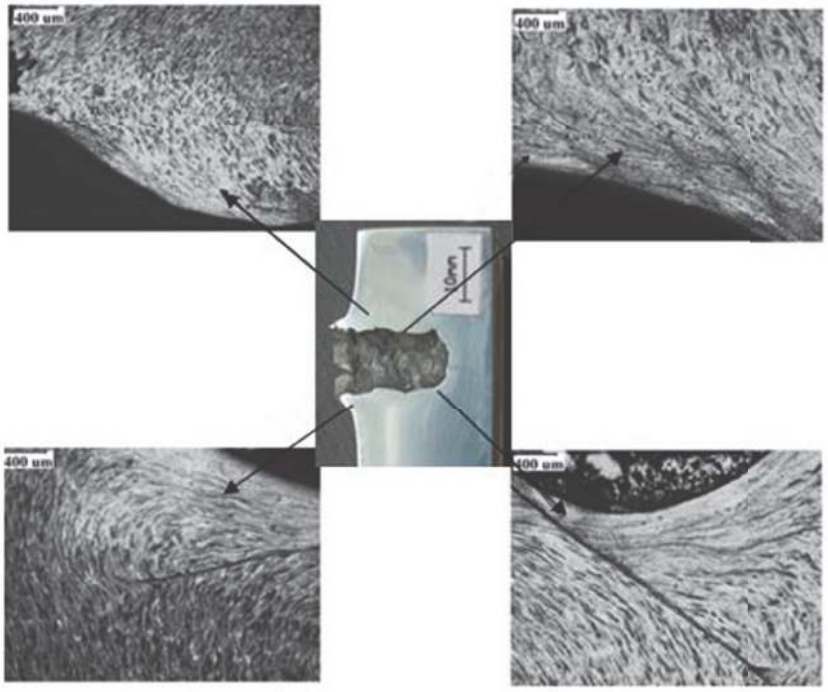

(b)

Fig.3.14: Post ballistic microstructures along the penetration channel impacted by soft steel projectile: (a) surface and (b) centre.

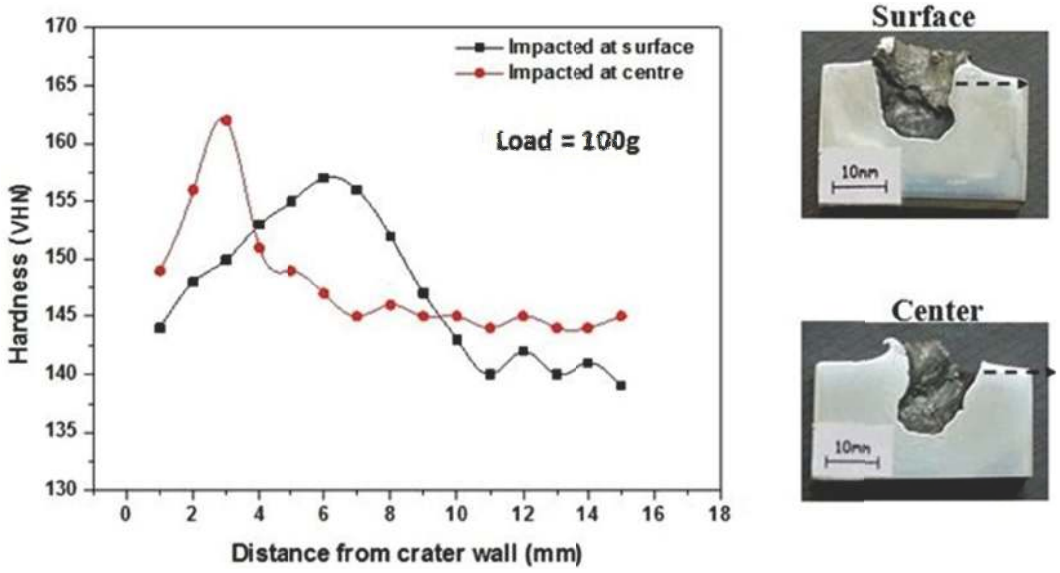

Fig. 3.15: Post ballistic micro-hardness measurements adjacent to the penetration channel wall.

case of the front face impacted targets, the peak in the hardness curve is seen at a distance of about 6 mm from the bottom of the penetration channel. For the targets impacted at the centre of the plate, the peak hardness is observed at a distance of about 3mm from the entrance point of projectile.

3.3. Discussion

The results from the optical microscopy clearly reflect a difference in microstructure at the surface and the centre of the plate. The relatively large volume fraction of recrystallized grains at the surface can be attributed to three factors. These are: (i) temperature gradients produced through the work piece created by heat transfer between the rolls and the work piece, (ii) strain gradients created by friction between the rolls and the work piece and (iii) redundant deformations contribute to this non-uniform microstructure(Chen et al., 2007). The recrystallization in present alloy has occurred around the prior deformed grains, wherein the precipitation of $Al_6(FeMn)$ and Mg_2Si occurs. This in

turn contributes to PSN. It is to be noted that the these precipitates are more finely distributed at the centre than that of the surface of the 70 mm AA 7017 plate (Fig 3.2 a, b]. This can again be attributed to temperature as well as strain gradient as mentioned above. It has been reported that the small dispersed particles in the matrix retard recrystallization rates through exerting a drag force on migrating grain or sub-grain boundaries and preventing the nucleation of recrystallization(Lang et al., 2011). This also explains the observation of less recrystallization at centre portion of the plate.

Both the XRD patterns from surface and centre of the plate exhibit different intensity ratios which are dissimilar to typical powder patterns of Al. This clearly indicates the presence of different texture at surface and centre of the plate. The overall intensity of ODF at the centre is more than seven times higher from the surface. The texture components observed at the surface are either recrystallisation component or located near recrystallisation components. This also reflects that the associated cooling rates after hot rolling is probably not sufficient to produce stable recrystallisation texture. On the other hand, the texture at the centre is quite sharp and close to typical Bs component. The corresponding β fibre also supports this observation. Therefore, the difference in texture at the surface and centre of the plate can therefore, be attributed to the stored energy, which drives the recrystallisation process. This is much higher at the surface than that of the centre.

It is observed that the mechanical properties also illustrate anisotropy at surface and centre. There is substantial difference in strength at centre than that at surface. The strength is usually dependent on both the texture and the microstructure, especially grain shape. The yield strength can generally be related to the critical resolved shear stress (CRSS) by an equation of the type (Chen et al., 2007):

$$\sigma_y = \Delta\sigma_{gb} + M\tau_{tot} \text{--------- 3.1}$$

where $\Delta\sigma_{gb}$ is the strength due to the grain shape, M the Taylor factor which depends on texture and τ_{tot} the CRSS of the grains. In the present study, centre of the plate shows more elongated grains than those at the surface. Such a behaviour can be attributed to relatively larger fraction of recrystallization at the surface than the centre. As mentioned earlier, recrystallization occurs in present alloy due to PSN. The recrystallised grains are equiaxed and the large fraction of recrystallized grains at the surface of the plate also reduces the

aspect ratios of unrecrystallized grains (Fig. 3.1). As a result, different aspect ratios of grains at the surface and centre of the plate result in different mechanical properties such as σ_{YS}, σ_{UTS}, bulk hardness, ductility and Charpy impact energy values. The difference is maximum in yield strength. It has been mentioned that the most affected property due to presence of texture is yield strength but the results of the present study indicate that the other properties are also getting influenced (Dieter, 1988; Lang et al., 2011).

As mentioned above, the yield strength contributed from the grain shape, i.e. $\Delta\sigma_{gb}$ is higher in the interior than on the surface. The texture is more than seven times sharper at the centre than at the surface, which has led to higher *M* value in the centre. Thus, due to the effects of both grain shape and texture, the centre of the plate displays large value of yield strength. As strength and toughness values are inversely proportional to each other, the centre of the plate with high strength shows lower ductility and impact toughness.

The difference in ductility and impact energy at surface and centre of the plate can also be explained from their respective fracture surfaces (Figs. 3.8-9). As mentioned above, cracks are formed within and around the Fe rich precipitates at the surface as well as centre of the plate for both tensile and Charpy broken samples. However, formation of cracks in the matrix at centre of the plate can be corroborated with a high intensity texture component located between $\{168\}\langle 211\rangle$ and Bs components. It has been mentioned that only four slip systems are activated for a material with an ideal Brass texture compressed along the short transverse direction (Chang et al., 1998). That clearly indicates the presence of limited number of active slip systems associated with Bs component. This has introduced an inhomogeneous deformation during ballistic impact at centre of the plate. As a result, cracks appeared in the matrix of the centre of the plate. On the other hand, cracks in matrix are absent at the surface due to moderate texture.

Presence of sharp texture in the centre portion of the plate can also be correlated with the presence of large fraction of shear bands at the centre of ballistically evaluated plates. The misorientations among neighbouring grains are relatively less at the centre due to presence of sharp texture. This reduces the effectiveness of the grain boundaries as a barrier to slip, which can easily propagate through the grain boundary into neighbouring

grains(Chang et al., 1998). As a result, a large fraction of shear bands are present at the centre of the plate.

For better ballistic performance of any armor material, it is essential that it should be able to absorb as much energy of the projectile as possible in a homogenous manner (Wingrove and Wulff, 1973; Bhat, 1985). Energy absorption in armor material takes place by plastic deformation which can be inferred from the post-ballistic damage patterns, microstructures and mirco-hardness observations adjacent to the penetration channel. Nice petalling damage pattern are observed on surface of the 70 mm AA 7017 plate after ballistic impact. This indicates the better ductility and toughness of the target. It also points out that the impact energy is getting transmitted to the adjacent regions effectively. Broken petal damage patterns observed at the centre indicate towards low ductility and impact toughness at centre. Also it points out that the impact energy is not uniformly getting transmitted to the adjacent regions.

From the post ballistic microstructural observations (Fig. 3.12-3.14), large deformations along with shear bands are observed in all the target plates. However, it is seen that on the surface impacted plates, both the shear band and crack formation decrease considerably. Formation of adiabatic shear bands at high strain rates at room temperature has been studied by several investigators (Timothy, 1987; Lee et al., 1995; Xue et al., 2004). During projectile impact, heat generated by the shear deformation is restricted to a narrow region in which it decreases the material strength and causes instability. Shear band is generated due to this extension of thermo-mechanical instability. The incompatibility of the deformed region increases to accommodate the overall distribution of dissipation energy. This results in cracks in surrounding regions. Hence, it can be inferred that formation of less number of shear bands at the surface of the plate indicates better dissipation of heat generated by the projectile impact. The plastic deformation is better distributed and more homogeneous if shear bands are not formed (Korbel et al., 1983). It is to be noted that both the surface and centre of the plate display moderate and very strong texture, respectively. This has resulted in different properties. Observations of less number of shear bands at plates impacted on the surface therefore suggest that the heat generated due to projectile impact has dissipated to the surrounding areas effectively due to moderate texture. On the other hand,

energy dissipation is non uniform at centre of the plate due to the presence of very strong texture. As a result, surface of the plate displays better ballistic performance than the centre.

The variation in hardness adjacent to the penetration channel is a result of two simultaneously competing processes i.e. annealing and strain hardening effects. Annealing effect caused by rise in temperature after projectile impact and strain hardening caused by severe deformation. Adjacent to the penetration channel, wall temperature rise is high. As a result, the hardness rise is less. Little beyond, annealing effect decreases but strain hardening is still there. This results in the increase in hardness. Eventually, the extent of strain hardening also decreases. Consequently, there is a fall in the hardness curve till it reaches the initial hardness of the plate. In case of surface impacted plates, the extent of deformation is spread over a comparatively larger volume than that of the plates impacted on the centre of the plate. This implies that more volume of the material at the surface is involved in absorbing the kinetic energy of the projectile. This in turn helps the material to absorb the energy in a homogeneous manner. The micro-hardness results are in accordance with the microstructural observations.

3.4. Conclusions

Microstructures and textures at surface and centre of the 70 mm AA 7017 plate are heterogeneous because of the different rate of recrystallization occurred through the plate thickness. The extent of elongation of grains is more at the centre than that of the surface. The overall strength of texture at the centre of the plate is nearly seven times larger than that at the surface. The different microstructures and textures at surface and centre of the plate give rise to the anisotropy of the mechanical properties. The strength and hardness are high at centre whereas both the ductility and impact toughness are more at the surface. The weak texture at surface helps the material to absorb the projectile impact energy efficiently and it has led to a better ballistic behaviour of the material. Due to strong texture at the centre of the material, the impact energy gets constricted to a narrow region and facilitates the formation of easy shear bands and a poor ballistic behaviour.